



Supplementary material

INDEX

1
2
3
4
5
6
7
8
9
10
11
12
13
14
15
16
17
18
19
20
21
22
23
24
25
26
27
28
29
30
31
32
33
34
35
36
37
38
39
40
41
42

1. Molecular dynamic methods.....Page 2.
2. Residues in BTL2 that were modified to create the quadruple mutant ccBTL2.....Page 4.
3. Figure S2. SDS-PAGE electrophoresis of BTL2 and ccBTL2 lipases.....Page 5.
4. Figure S3. Effect of the acyl length on the hydrolysis of *p*-nitrophenyl esters with immobilized BTL2 and ccBTL2 applying different redox pretreatments.....Page 6.
5. Figure S4. Reference volumes used to monitor the variation between the crystallographic structures of BTL2 and the ccBTL2 modelPage 7.
6. References.....Page 8.

43 1. Molecular dynamics methods.

44 The crystallographic structure of the BTL2 in open conformation (UniProtKB - Q59260) was obtained
45 from the RCSB-Protein Data Bank (PDB code: 2W22). In order to prepare the structures for further
46 simulations, water molecules and co-solvent molecules including both Triton X-100 molecules (EGC-
47 403 and ECG-404) (Fig. S4) were removed. Next, we built a homology model of the BTL2 in the closed
48 conformation using as template the *Bacillus stearothermophilus* lipase 1 (UniProtKB - Q9L6D3, PDB
49 code: 1JI3) with a sequence homology of 95.1%. This homology model was built with the SWISS-
50 MODEL web server [1] obtaining a positive QMEAN value [2] of 0.66. The protonation states were
51 calculated for both structures using the H++ web server [3] which relies on AMBER parameters and
52 finite difference solutions to the Poisson–Boltzmann equation.

53 The conformational change from the closed to the open conformation was simulated using targeted
54 molecular dynamics (TMD) as implemented in AMBER 16 [4], using the previously generated
55 models. A salt concentration of 0.15 M and an internal and external dielectric constant of 4 and 80,
56 respectively, were used. Atom types and charges were assigned according to AMBER ff15FB (Force
57 Balance) force field [5]. Both systems were hydrated by using boxes containing explicit TIP3PFB water
58 molecules [6] with added counter ions to maintain electro neutrality. Solvent molecules and counter
59 ions were relaxed by energy minimization and then allowed to redistribute around the positional
60 restrained structures during a 50 ps run at constant temperature (300 K) and pressure (1 atm). These
61 initial harmonic restraints were gradually reduced in a series of progressive energy minimizations
62 steps until they were completely removed. The resulting systems were heated again from 100 to 300
63 K during 20 ps and allowed to equilibrate in the absence of any restraints for 1.0 ns during which the
64 system coordinates were collected every 2 ps for further analysis. The equilibrated structures were
65 then used as the starting points for the three targeted MD simulations we ran. These simulations had
66 a duration of 5, 10 and 50 ns applying a steering force based on a mass-weighted RMSD with respect
67 to reference target conformation with force constants of 1, 0.75 and 0.5. Periodic boundary conditions
68 and the Particle Mesh Ewald methods were used to treat long-range electrostatic effects. The SHAKE
69 algorithm [7] was used throughout; applied to all bonds and an integration step of 2.0 fs.

70 The Root mean square deviation of the c-alpha atoms (RMSD) was calculated and distances between
71 A191 and F206 where measured along the TMD simulation with the help of ccptraaj tool from
72 Ambertools 14 [8]. Moreover, from each of the three trajectories, we selected a structure when
73 residues A191 and F206 where at least at 5 Å from each other; these structures were conformationally
74 similar to the open conformation. Then, we built three ccBTL2 structures using the mutagenesis tool
75 from PyMOL Molecular Graphics [9] and performed an energy minimization, which led to three
76 highly similar models.

77 Finally, we performed molecular dynamic (MD) simulations on the ccBTL2, BTL2 open and closed
78 conformations, in the absence of ligands using the previously generated molecular systems and
79 AMBER16. The AMBER force field ff15FB (Force Balance) for the protein parametrization was
80 applied. Water and metal parameters were obtained from the TIP3PFB and ions parameter
81 modification file. After that, systems were minimized in vacuum, in order to release possible
82 undesired interactions or clashes. Then the systems were embedded in an TIP3FB water box of
83 approximately 12000 water molecules forcing neutrality by adding chloride ions. Initially, the

84 embedded systems were minimized and heated to 300 K in a NVT ensemble followed by
85 equilibration during 0.5 ns in a NPT ensemble. In all systems the hydrogen atoms were kept at their
86 equilibrium distance by means of the SHAKE algorithm. Atom pair distance cutoffs were applied at
87 10.0 Angstroms to compute the Van der Waals interactions, while long-range electrostatics were
88 computed by means of Particle-Mesh Ewald (PME) method [10]. Finally, the MD simulation was
89 performed up to 200 ns using the thermostat NPT ensemble at 300 K and generating snapshots each
90 20 ps for further analysis of both systems (10 000 in total). The trajectories of all complexes were
91 collected and analyzed by the cpptraj module of AMBER16 [8] in order to obtain the previously
92 mentioned root mean square deviation of the overall c-alpha atoms, and the atoms from alpha6- and
93 alpha7-helices. Moreover, 10000 aligned PDBs were obtained from each trajectory to perform the
94 analysis of the active pocket cavity by the versatile Fpocket software [11], which is based on Voronoi
95 tessellation algorithm. The Mdpocket module [12] was applied to obtain the corresponding volumes
96 in each MD simulation step using as a pocket reference (pocket1 and pocket2) the first ones obtained
97 from the first step (md0) in the initial BTL2 in the open conformation. The volume of the pockets
98 recorded along the simulation where represented as trend lines and *violin* plots using the software
99 RStudio (www.rstudio.org) and the package ggplot2.

100
101
102
103
104
105
106
107
108
109
110
111
112
113
114
115
116
117
118
119
120
121
122
123
124
125

126
127
128
129
130
131
132
133
134
135
136
137
138
139
140
141
142
143
144
145
146
147
148
149
150
151
152
153
154
155
156
157
158
159
160
161
162
163
164
165
166
167
168

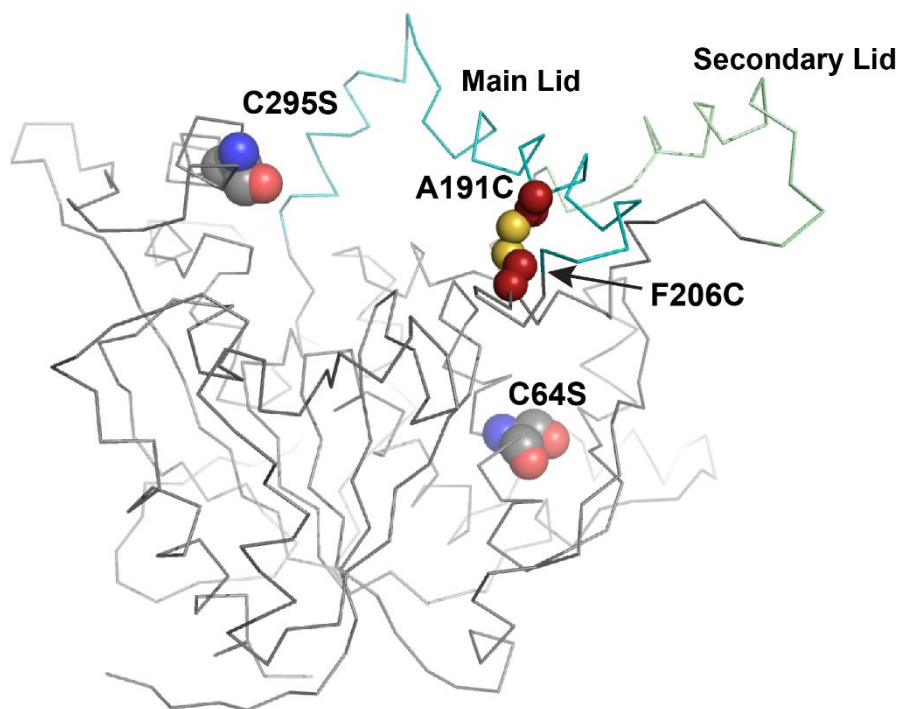


Figure S1. Residues in BTL2 that were modified to create the quadruple mutant *ccBTL2*.

169
170
171
172
173
174
175
176
177
178
179
180
181
182
183
184
185
186
187
188
189
190
191
192
193
194
195
196
197
198
199
200
201
202
203
204
205
206
207
208
209
210
211

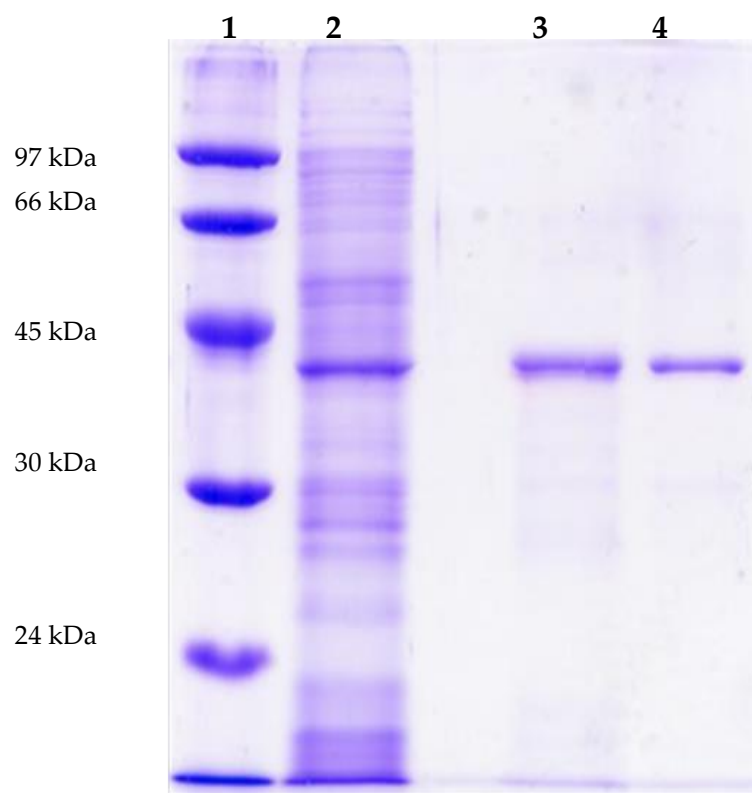


Figure S2. SDS-PAGE electrophoresis of BTL2 and ccBTL2 lipases. From left to right: Lane 1 (Molecular weight markers); Lane 2 crude extract from *E. coli* expressing ccBTL2; Lane 3 purified ccBTL2; Lane 4 purified BTL2.

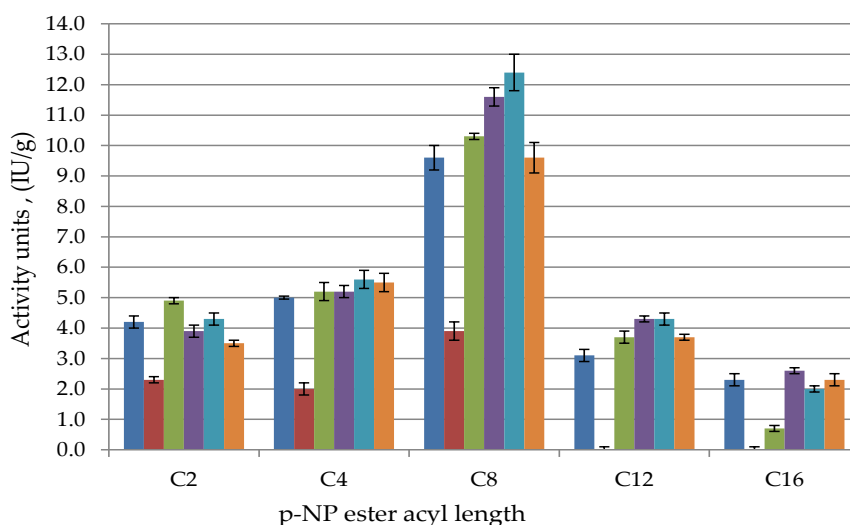
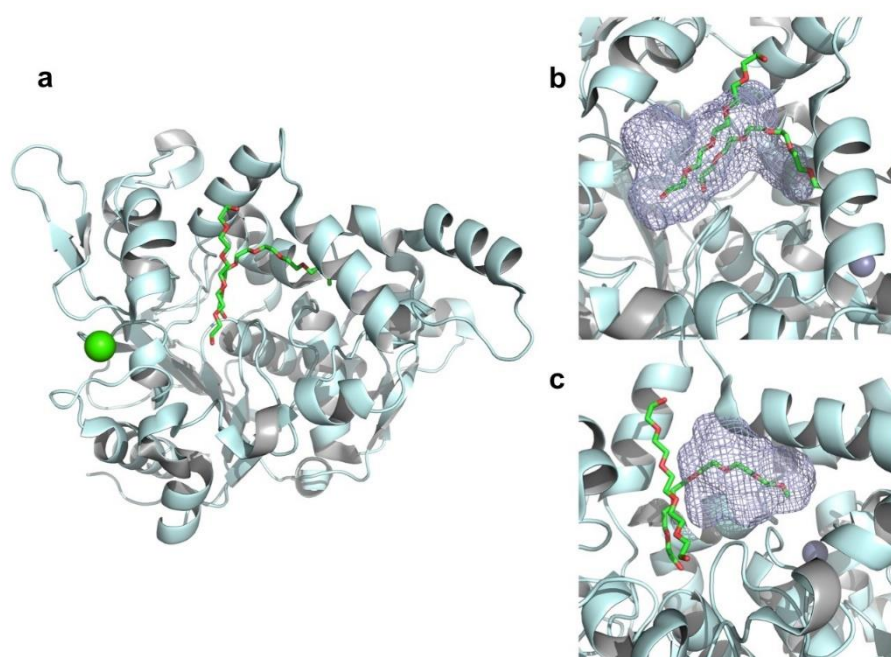


Figure S3. Hydrolysis of *p*-NP esters of different acyl chain length with immobilized *wt*BTL2 and *cc*BTL2 with different redox pretreatments. BTL2-CNBr: as obtained from purification (blue bar), pretreated with 200 mM Cu²⁺ (red bar), pretreated with 25 mM DTT (green bar). *cc*BTL2-CNBr: as obtained from purification (purple bar), pretreated with 200 mM Cu²⁺ (cyan bar), pretreated with 25 mM DTT (orange bar).

Note S1: For both CNBr derivatives made with lipase without any pretreatment, there are not significant differences on hydrolytic activity (Figure 4) except for the C8 ester where *cc*BTL2-CNBr is 18,8 % (11.4 IU/g) higher than that of the BTL2 derivative (9,6 IU/g). The profile obtained for the BTL2 derivative activity vs. *p*-NP ester length chain is close to that obtained for the free BTL2 enzyme. It is noteworthy that both BTL2 and *cc*BTL2 showed broad substrate specificity towards *p*-NP acyl esters of different length, processing chains from C2 up to C16. Nevertheless, it was also obvious the relative higher activity against the C8 ester (Ref. [22] in the main text). The oxidative pretreatment deteriorates BTL2 derivative activity especially with C12 and C16 *p*-NP esters while for the *cc*BTL2 the same pretreatment was slightly positive or neutral. In general, the hydrolytic behavior of the *cc*BTL2 derivative surpasses that of BTL2 even after the harsh oxidizing conditions assayed in presence of Cu²⁺.

249



250

251 **Figure S4.** Reference volumes used to monitor the variation between the crystallographic
252 structures of BTL2 and the ccBTL2 model. a) Crystallographic structure of BTL2 (open conformation)
253 in complex with Triton X-100 (EGC-403 and EGC-404) moieties (PDB code: 2W22). b) Volumetric
254 representation (gray mesh) of Pocket 1 fitting the EGC-404 molecule. c) Volumetric representation
255 (gray mesh) of Pocket 2 fitting the EGC-403 molecule.

256

257

258

259

260

261

262

263

264

265

266

267

268

269

270

271

272

273

274

275

276

277 **References**

- 278 1. Waterhouse, A.; Bertoni, M.; Bienert, S.; Studer, G.; Tauriello, G.; Gumienny, R.; Heer, F.T.; de Beer,
279 T.A.P.; Rempfer, C.; Bordoli, L.; et al. SWISS-MODEL: homology modelling of protein structures and
280 complexes. *Nucleic Acids Research* **2018**, *46*, W296–W303.
- 281 2. Benkert, P.; Biasini, M.; Schwede, T. Toward the estimation of the absolute quality of individual protein
282 structure models. *Bioinformatics* **2011**, *27*, 343–350.
- 283 3. Gordon, J.C.; Myers, J.B.; Folta, T.; Shoja, V.; Heath, L.S.; Onufriev, A. H++: a server for estimating pKas
284 and adding missing hydrogens to macromolecules. *Nucleic Acids Research* **2005**, *33*, W368–W371.
- 285 4. D.A. Case, R.M. Betz, D.S. Cerutti, T.E. Cheatham, III, T.A. Darden, R.E. Duke, T.J. Giese, H.G.; A.W.
286 Goetz, N. Homeyer, S. Izadi, P. Janowski, J. Kaus, A. Kovalenko, T.S. Lee, S. LeGrand, P. Li, C.; Lin, T.
287 Luchko, R. Luo, B. Madej, D. Mermelstein, K.M. Merz, G. Monard, H. Nguyen, H.T. Nguyen, I.
288 Omelyan, A. Onufriev, D.R. Roe, A. Roitberg, C. Sagui, C.L. Simmerling, W.M. Botello-Smith, J.S.; R.C.
289 Walker, J. Wang, R.M. Wolf, X. Wu, L.X. and P.A.K. (2016) AMBER 2016. University of California, San
290 Francisco.
- 291 5. Wang, L.-P.; McKiernan, K.A.; Gomes, J.; Beauchamp, K.A.; Head-Gordon, T.; Rice, J.E.; Swope, W.C.;
292 Martínez, T.J.; Pande, V.S. Building a More Predictive Protein Force Field: A Systematic and
293 Reproducible Route to AMBER-FB15. *The Journal of Physical Chemistry B* **2017**, *121*, 4023–4039.
- 294 6. Wang, L.-P.; Martinez, T.J.; Pande, V.S. Building Force Fields: An Automatic, Systematic, and
295 Reproducible Approach. *The Journal of Physical Chemistry Letters* **2014**, *5*, 1885–1891.
- 296 7. Ryckaert, J.P.; Ciccotti, G.; Berendsen, H.J.C. Numerical integration of the cartesian equations of motion
297 of a system with constraints: molecular dynamics of n-alkanes. *Journal of Computational Physics* **1977**, *23*,
298 327–341.
- 299 8. Roe, D.R.; Cheatham, T.E. PTRAJ and CPPTRAJ: Software for processing and analysis of molecular
300 dynamics trajectory data. *Journal of Chemical Theory and Computation* **2013**, *9*, 3084–3095.
- 301 9. L DeLano, W. Pymol: An open-source molecular graphics tool. *{CCP4} Newsletter On Protein*
302 *Crystallography* **2002**, *40*.
- 303 10. Darden, T.; York, D.; Pedersen, L. Particle mesh Ewald: An N·log(N) method for Ewald sums in large
304 systems. *The Journal of Chemical Physics* **1993**, *98*, 10089–10092.
- 305 11. Le Guilloux, V.; Schmidtke, P.; Tuffery, P. Fpocket: An open source platform for ligand pocket detection.
306 *BMC Bioinformatics* **2009**, *10*, 168.
- 307 12. Schmidtke, P.; Bidon-Chanal, A.; Luque, F.J.; Barril, X. MDpocket: open-source cavity detection and
308 characterization on molecular dynamics trajectories. *Bioinformatics* **2011**, *27*, 3276–3285.

309

310

311

312



© 2019 by the authors. Submitted for possible open access publication under the terms and conditions of the Creative Commons Attribution (CC BY) license (<http://creativecommons.org/licenses/by/4.0/>).

313